Turkish Journal of Electrical Engineering & Computer Sciences

http://journals.tubitak.gov.tr/elektrik/

Research Article

Turk J Elec Eng & Comp Sci
(2019) 27: 4756 – 4767

doi:10.3906/elk-1903-194

Quantification of resistive wall instability for particle accelerator machines

Fatih YAMAN*
Department of Electrical and Electronics Engineering, Faculty of Engineering, İzmir Institute of Technology, İzmir, Turkey

Received: 31.03.2019 • **Accepted/Published Online:** 13.07.2019 • **Final Version:** 26.11.2019

Abstract: The aim of this study is to quantify longitudinal resistive wall impedances, corresponding wake functions, and wake potentials for different accelerator machines of interest. Accurate calculations of wake potentials by particle-in-cell codes are extremely difficult for the investigated parameters; therefore, we use an analytical approach and consider large domains with fine discretization for the required numerical integrations. The semianalytical wake potential computations are benchmarked against numerical general purpose 2D/3D Maxwell solver software codes and a different analytical approach for a certain set of parameters. We report examples to illustrate limitations of wake potential estimations from coupling impedances, and computations for the machines using realistic beam parameters and machine conditions. A numerical example where the aim is to find the wake potential of the machine from the 5% noisy impedance data is given.

Key words: Wake potential, resistive wall impedance, medium-β long bunches

1. Introduction

In particle accelerators, the coupling impedance is used to define the electromagnetic interaction of the particle beam with its environment. To operate the machine efficiently it is important to minimize the coupling impedance, otherwise it may cause unwanted effects like emittance growth or even beam losses due to instabilities, changes of the beam trajectory, and increase of the vacuum pressure. Discontinuities of the beam pipe due to various technical accelerator components (RF cavities, collimators, kickers etc.), existence of electron cloud effects, and the nonzero resistivity of the pipe wall are the main sources of impedances in particle accelerators and storage rings [1, 2].

The main physical components of the impedances are the space charge impedance, which is caused by the bunch distribution and resistive wall impedance which is related to the medium parameters of the wall. In this study we omit the space charge impedance calculations and focus on the numerical evaluations of resistive wall impedance and wake representations which can be used for micrometer/millimeter length short bunches up to long bunches in order of meters, and can be applied to ultrarelativistic ($\beta \approx 1$) and low-β ($\beta \approx 0.07$) machines, with $\beta = \upsilon/\mathbf{c}$ where υ is the beam velocity, c is the speed of light. In our numerical examples we consider low and medium-β long bunches e.g., $\sigma_z = 0.5m, 1m$ which are in the parameter scope of some operational machines, SNS, JPARC, SIS18, PS, and ECR.

Impedance calculations for nonultrarelativistic cases have been performed by Laslett et al. [3], Gluckstern [4], Zimmermann and Oide [5, 6], Al-khateeb et al. [7], Mounet [8] are well known studies in this area. Numerical

*Correspondence: fatihyaman@iyte.edu.tr

calculations of impedance and wake functions based on the Zimmermann–Oide model are presented by Quatraro and Rumolo [9], see also [10]. Furthermore, the impedance of thick vs. thin beam pipes was obtained by Hänichen et al. [11], by applying the Leontovich boundary condition [12] and in comparison with CST impedance simulations for the ultrarelativistic beams. Zannini et al. [13] discussed the possibility and the limitations of obtaining longitudinal and transverse impedances via CST 3D electromagnetic simulations by subtracting the analytically/numerically calculated direct space charge impedance contributions. Macridin et al. [14] calculated numerically the longitudinal and transverse impedances and wake functions in circular chambers for monopole and dipole channels. Note that those channels are the modes excited individually by the lowest order multipolar components of the beam current, e.g., $m = 0$ and $m = 1$ correspond to monopole and dipole channels, respectively for $\exp(im\theta)$ expansion of the fields in axially symmetyric geometries, for θ angular variation [1]. The numerical calculations of the longitudinal and transverse wall-impedances of multilayer axisymmetric or flat structures having finite wall thickness in ImpedanceWake2D [8] code. For more detailed information on beam instabilities we refer to the review by Métral et al. [15].

Wake potential calculations for very long/short bunch lengths using the particle-in-cell–based software bring a heavy computational load and accuracy issues. In order to treat such problems, Zagorodnov et al. [16] proposed an implicit scheme for the calculation of electromagnetic fields in the vicinity of short electron bunches for perfectly electric conductor boundaries and improved their algorithm in [17] so that the new accurate scheme does not use extended stencils. On the other hand, unlike the ultrarelativistic case, the space charge impedance dominates the coupling impedance in the calculation region for nonrelativistic bunches. For this reason, those codes that calculate first the EM-fields, and then postprocess the wakes have strong limitations in distinguishing resistive wall impedances from the total impedance [13]. Therefore, a promising approach to compute the wake potential of circular cylindrical beam pipe structures in extreme conditions is based on fundamental analytical calculations.

In this manuscript we are interested in the calculation of the longitudinal monopole impedance $Z_{||}^{(0)}$ via the Al-khateeb et al.'s [7] approach, since this mode has a stronger accelerating or decelerating effect on the beam compared to the higher-order modes, and it is very relevant for our parameter space. Once the longitudinal impedance is calculated, the transverse dipole impedance $Z_{\perp}^{(1)}$, which may deflect the beam, can be obtained from the given monopole impedance via the approximate generalized result presented in [4] as

$$Z_{\perp}^{(1)} = \frac{2}{k\, b^2}\, Z_{||}^{(0)}\,, \tag{1}$$

where k is the wave number and b is the radius of the beam pipe. It is generally accepted that the most important modes for the beam stability calculations are the monopole and dipole modes with lowest mode numbers [1]. In a following step, we obtain the wake function by a Fourier transformation. Afterwards the convolution integral is calculated numerically by considering Gaussian shaped bunched beams for machines having different velocity, beam pipe, electrical conductivity, and bunch lengths.

The structure of the paper is as follows, the longitudinal resistive wall impedance problem, and the analytical impedance models for the solution and the parameter scope of the numerical investigations, are introduced in the next section. Section 3 is devoted to the detailed investigations of impedance and wake function results. The following section focuses on the verification and comparison of wake potential results for the different machines. In the final section, conclusions and concluding remarks are presented.

2. Impedance model and parameters

We consider a uniformly charged, relatively small disk beam with radius a, which travels with a constant longitudinal velocity υ in the center of a cylindrical beam pipe with circular cross-section, having no discontinuities, and is arranged as a ring accelerator of circumference L.

The walls have a finite surface impedance Z_m, given as

$$Z_m = \frac{1+i}{\sigma\delta_s}\,, \qquad \delta_s = \sqrt{\frac{2}{\mu\omega\sigma}}\,, \tag{2}$$

in terms of skin depth δ_s which is a function of the permeability $\mu = \mu_0\mu_r$ of the material, frequency $\omega = 2\pi f$, and a constant conductivity σ, see [7].

The problem here is to find an expression for the resistive wall coupling impedance for this configuration via field matching which is valid for all frequencies. For this aim we consider the Al-khateeb et al. model [7] for the numerical calculations of the longitudinal monopole impedances, $Z_{||}^{(0)}$. Furthermore, we compare this model with the Macridin et al. approach [14] by considering the fact that the resistive wall impedances for two different source terms should be numerically equal even they have different representation, see [18]. Each impedance model has a different type of source terms, for instance in [7] the charge density is considered as a uniform disk source

$$\rho_c = \widetilde{\rho_c}(r,\theta)\delta(z-\upsilon t)\,, \tag{3}$$

whereas in [14] the charge density for a particle that moves through a circular chamber is decomposed in terms of multiple moments

$$\rho_c = \sum_{m=0}^{\infty} \frac{P_m\,\cos m\theta}{\pi\, a^{m+1}\,(1+\delta_{m,0})}\,\delta(r-a)\delta(z-\upsilon t)\,, \quad \left\{ \begin{array}{ll} \delta_{m,0}=1, & m=0 \\ \delta_{m,0}=0, & m\neq 0 \end{array} \right. , \tag{4}$$

where $P_m = Q\,a^m$ is the m^{th} multipole moment.

In Al-khateeb et al.'s model, the nonhomogeneous wave equation is given in terms of electric $\mathbf{E}$, and magnetic $\mathbf{B}$, fields as

$$\begin{aligned} \Delta\mathbf{E} - \frac{1}{c^2}\frac{\partial^2\mathbf{E}}{\partial t^2} &= \mu_0\frac{\partial\mathbf{J}}{\partial t} + \frac{\nabla\rho_c}{\epsilon_0}\,, \\ \Delta\mathbf{B} - \frac{1}{c^2}\frac{\partial^2\mathbf{B}}{\partial t^2} &= -\mu_0\nabla\times\mathbf{J}\,. \end{aligned} \tag{5}$$

Here the current density $\mathbf{J}$,

$$\mathbf{J} = \rho_c\,\boldsymbol{\upsilon} = \widetilde{\rho_c}(r,\theta)\,\beta c\,\delta(z-\upsilon t)\,\mathbf{z}\,, \tag{6}$$

is defined such that the continuity equation

$$\frac{\partial\rho_c}{\partial t} + \nabla\cdot\mathbf{J} = 0 \tag{7}$$

is satisfied. The relativistic factor β in (6) is related to the Lorentz factor γ, via $\gamma = 1/\sqrt{1-\beta^2}$.

The electric field is obtained analytically via field matching in the frequency domain by taking the Fourier transform of the equation (5) and applying the proposed boundary conditions inside the beam pipe. We refer

[7] for the detailed derivations of the fields and the impedance. Accordingly the z-component of the electric field is represented in cylindrical coordinates

$$E_z(r,z,\omega) = \frac{Q\,e^{ikz}}{\pi a \epsilon_0 \gamma \beta c} \begin{cases} \widetilde{p}\, I_1(k_r a) I_0(k_r r) - i I_1(k_r a) K_0(k_r r), & r > a \\ \widetilde{p}\, I_1(k_r a) I_0(k_r r) + i K_1(k_r a) I_0(k_r r) - \dfrac{i}{k_r a}, & r \le a \end{cases} , \tag{8}$$

where

$$\widetilde{p} = \frac{(\beta\gamma Z_m / c\mu_0) K_1(k_r\, b) + i\, K_0(k_r b)}{I_0(k_r b) + i(\beta\gamma Z_m / c\mu_0) I_1(k_r b)} ,$$

$Q = \rho_c \pi a^2$ is the total charge distributed uniformly on the surface of an infinitely thin disk of radius a, I_j and K_j $(j = 0, 1)$ are the $j-$th order modified Bessel functions and $k_r = \omega/\gamma\beta c$. Afterwards the coupling impedance is calculated via the formal definition,

$$Z_{||}(r\,,\omega) = \frac{1}{Q^2} \int_{V_{beam}} d^3 r'\, E_z(r', z, \omega)\, j^*(r', z, \omega)\,, \tag{9}$$

using the complex conjugate of the electrical current density $j^*(r', z, \omega) = \rho_c e^{-ikz}$. This coupling impedance representation contains both space charge and resistive wall impedances. In particular the resistive wall impedance at $r = a$ which we are interested in can be calculated as

$$Z^{(0)}_{||\,,\mathrm{RW}}(a\,,\omega) = 2L\, \frac{I_1^2(k_r\, a)}{\pi a^2 \epsilon_0 \omega} \left[\widetilde{p} - i \frac{K_0(k_r b)}{I_0(k_r b)} \right] . \tag{10}$$

In Macridin et al.'s model [14], Maxwell's equations are solved with the help of auxiliary electric Φ, and magnetic vector $\mathbf{A}$ potentials such that the fields are obtained analytically via the following relations

$$\begin{aligned} \mathbf{E} &= -\nabla\, \Phi - \frac{\partial \mathbf{A}}{\partial t}\,, \\ Z_0 \mathbf{H} &= c\, \nabla \times \mathbf{A}\,, \end{aligned} \tag{11}$$

where $Z_0 = 120\pi\,\Omega$. The longitudinal monopole $(m = 0)$ impedance at the beam surface $r = a$ is calculated as

$$Z^{(M)}_{||\,,RW}(a\,,\omega) = \frac{Z_m}{2\pi b} \frac{I_0^2(k_r\, a)}{I_0(k_r\, b) \left[I_0(k_r\, b) + i\beta\gamma \frac{Z_m}{Z_0} I_1(k_r\, b) \right]} . \tag{12}$$

In this study we focus on the machine parameters of an accumulator ring such as those used at the Spallation Neutron Source (SNS), the synchrotron of the Japan Proton Accelerator Research Complex (JPARC), the booster rings of the CERN Proton Synchrotron (PS), the electron-cyclotron resonance ion source (ECR), and the GSI heavy-ion-synchrotron (SIS18), see [5, 10, 19–22].

Among those parameters listed in Table 1, E_k corresponds to the kinetic energy per proton and N_p the number of protons/ions per bunch.

For the radius of SNS beam, the variation of space charge impedance, which is basically the difference between Eq. 10 and Eq. 9, with respect to $\beta - function$ is considered. The value of the $\beta - function$ is picked

Table 1. Parameters employed for the simulations.

	SNS	JPARC	PS	ECR	SIS18
β	0.875	0.699	0.519	0.077	0.866
$E_k(MeV)$	1001.19	374.29	159.63	2.79	939.40
$\sigma(S/m)$	1.30×10^6	1.40×10^6	1×10^6	1.40×10^6	1×10^6
$a(cm)$	1.84	2	0.3	0.4	1
$b(cm)$	10	12.5	8	3	5
N_p	1.5×10^{14}	4×10^{13}	1.2×10^{12}	2×10^{13}	4×10^9

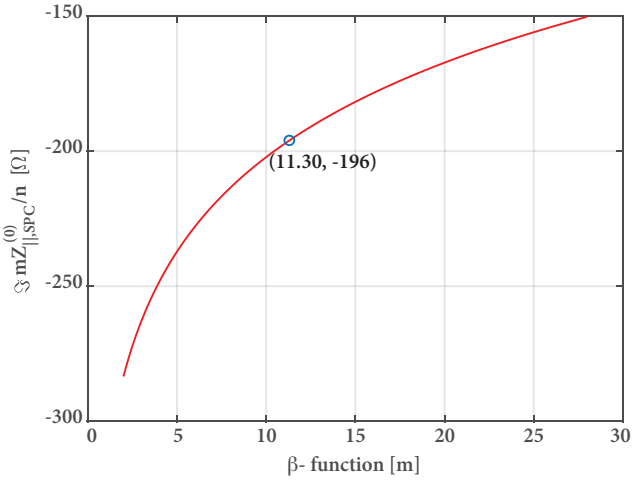

Figure 1. Space charge impedance for SNS employing Al-khateeb et al.'s model.

from Figure 1 such that the space charge impedance can be read as it was reported in [19]. Afterwards, the radius is found from the given approximate emittance value $30\,\pi$ mm-mrad of SNS [20, 23] at the revolution frequency 1.058 MHz, where n is the harmonic number. We note that the resistive wall impedance $Z^{(0)}_{||,\mathrm{RW}} = 0.707(1+i)$ can be calculated as it was presented in [19] via substitution of the reconstructed beam radius $a = 1.84$ cm to the impedance equation Eq. 10 at the revolution frequency.

3. Resistive wall impedance calculations

This section illustrates the variation of the resistive wall impedance vs. frequency for different accelerators. Convergence behavior of the numerical results, absolute value of maximum impedance per meter and corresponding frequencies are listed as a table. The last part of this section is devoted to investigate and discuss the wake functions of machines.

Figure 2a shows a typical behavior of the coupling impedance for a selected machine SNS where the maximum value of the impedance obtained is $\approx 0.076\,[\Omega m^{-1}]$ at around 630 MHz. Furthermore, the figure emphasizes good agreement of the results obtained via two different models.

Figure 2b shows the real and imaginary parts of the resistive wall impedance wrt. frequency for the different machines, based on Al-Khateeb et al.'s model. The solid lines in this graph represent the real parts of the impedances and the dashed lines on each curve correspond to the imaginary parts. It can be seen from Figure 2b that solid and dashed lines are on top of each other which means that real and imaginary parts

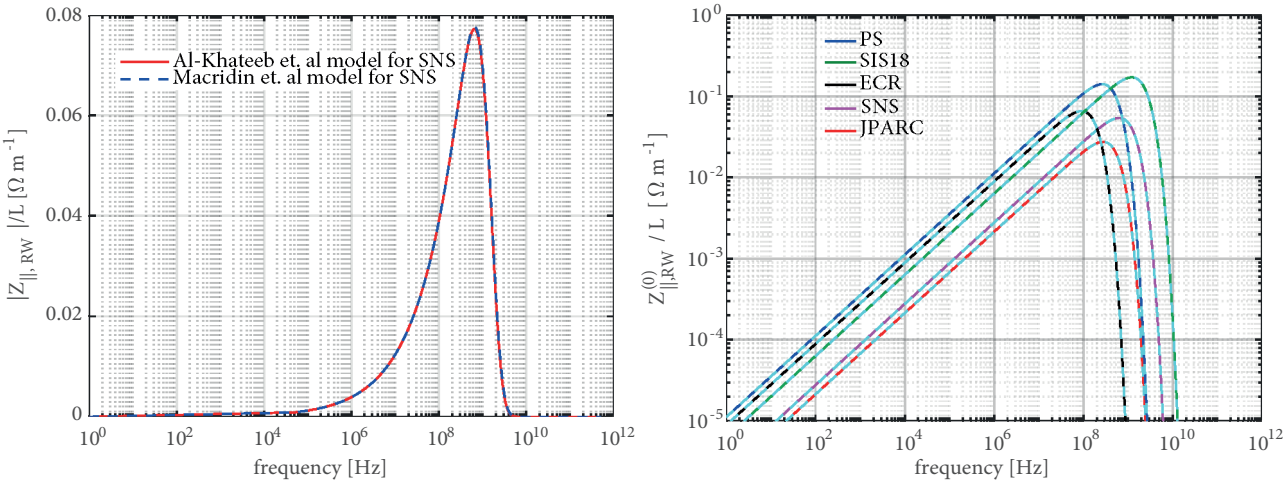

(a) SNS impedance (b) Impedances for different machines

Figure 2. Resistive wall Impedance Calculations (a) with two models for SNS (b) with Al-Khateeb et al.'s model (dashed lines correspond to imaginary parts of the impedance).

are equal for $k_z\delta_s \ll 2/\beta^2\gamma$ as it is expected from the theory [7] where $k_z = \omega/v$ is the wave number in the direction of propagation. This agreement on the results could be considered as a theoretical verification of our numerical calculations.

It is observed that the impedances reach their peak value at frequencies $>$ 80 MHz, and decrease substantially at higher frequencies, $\approx$ 10 GHz, under the given parameters. The peak value of the absolute impedance and the corresponding frequency along with the convergence behavior of the computation is listed in Table 2.

Table 2. Convergence study for impedance calculations using different machines N_f: discretization number for the frequency f:frequency and $\bar{Z} = |max(Z_{||,RW})|/L$: absolute value of maximum impedance per length.

	ECR		JPARC		PS		SIS18		SNS	
N_f	f[GHz]	$\bar{Z}[\Omega m^{-1}]$	f[GHz]	$\bar{Z}[\Omega m^{-1}]$	f[GHz]	$\bar{Z}[\Omega m^{-1}]$	f[GHz]	$\bar{Z}[\Omega m^{-1}]$	f[GHz]	$\bar{Z}[\Omega m^{-1}]$
$1e3$	0.100	0.09186090	0.300	0.03844316	0.300	0.19709021	1.000	0.23656373	0.500	0.07441583
$1e4$	0.090	0.09236873	0.270	0.03860934	0.260	0.19865575	1.200	0.24012371	0.650	0.07603414
$1e5$	0.090	0.09236873	0.273	0.03861173	0.264	0.19868241	1.210	0.24012718	0.630	0.07606971
$1e6$	0.090	0.09236874	0.273	0.03861174	0.264	0.19868271	1.207	0.24012777	0.630	0.07606971
$1e7$	0.090	0.09236874	0.273	0.03861174	0.264	0.19868271	1.207	0.24012777	0.630	0.07606971

In this table, the consistency of the impedance results obtained via two different models is illustrated in a more clear form. Accordingly, we chose Al-Khateeb et al.'s model for the wake calculations in the rest of the paper.

4. Wake function results

The longitudinal wake function $G^{(0)}_{||,\mathrm{RW}}$, which can be considered as the response of a structure to an infinitely short bunch is calculated via the Fourier integral,

$$G^{(0)}_{||,\mathrm{RW}}(z) = \frac{1}{2\pi}\int_{-\infty}^{\infty} d\omega\, Z^{(0)}_{||,\mathrm{RW}}(\omega)\, e^{-i\frac{\omega}{\beta c}}\,. \tag{13}$$

By considering the analogy with Green's functions, they can be viewed as part of the convolution with finite length bunches of the wake potential. At this point, it is worth to mention that accurate numerical computations of wake functions require large integration domains, where significant numerical difficulties may occur in the numerical calculations.

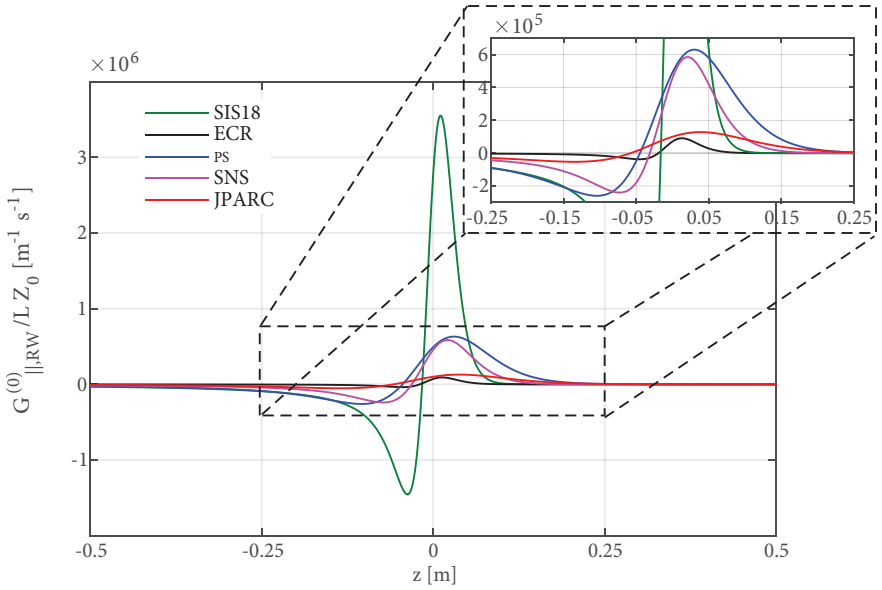

Figure 3. Wake function calculations.

In Figure 3 the wake functions, normalized to the length times the free space wave impedance (LZ_0) for the machines of practical interest, are given. As a first result, we observed that the longitudinal fields excited by the beam in front of the leading particles are not negligible for nonultrarelativistic beams [9]. Additionally, the SIS18 wake function shows to be dominant in this comparison, while those of the PS and the SNS are similar. These observations are difficult to predict from the impedance vs. frequency plots, or the data listed in Table 2. For example, the normalized maximum impedance value appears at ≈ 260 MHz as $\approx 0.198[\Omega m^{-1}]$ for the PS, and at ≈ 630 MHz as $\approx 0.076[\Omega m^{-1}]$ for the SNS, even though both machines have similar wake functions. On the other hand, this wake function consistency does not guarantee similar wake potential values, see the factor ≈ 10 difference in wake potential magnitudes between the PS and the SNS in the corresponding figures of the following section. Hence, one needs to calculate both, the wake functions and the wake potentials accurately.

5. Wake potential calculations for the machines

Resistive wall wake potentials can be obtained from convolution integrals of the wake functions for the considered Gaussian bunches via

$$W(\tau) = \frac{1}{\sqrt{2\pi}\sigma_z} \int_0^\infty dt\, G^{(0)}_{||,\mathrm{RW}}(t) \exp\left[-\frac{(\tau - t)^2}{2\sigma_z^2}\right], \tag{14}$$

where $G^{(0)}_{||,\mathrm{RW}}$ is the related longitudinal wake function and σ_z is the bunch length. For the wake potentials the main difficulty appears in the numerical computation of the convolution integral for very short wake functions, stimulated by rather long bunches. In this section, we first present a benchmark result of our quasianalytical calculations with existing commercial (CST) and freely downloadable codes (ECHOz) as well

as with an analytical study. For the benchmark, the beam and machine parameters are considered as $\beta \approx 1$, $\sigma_z = 1mm$, $a \approx 0$, $b = 1cm$, $\sigma = 100S/m$. The resistive wall wake potential calculations are compared with the analytical approach of Zagorodnov–Dohlus [24], the Zagorodnov's ECHOz code [25], and the CST [1]-WaK Solver, shown in Figure 4. Note that ECHOz has several subversions and we use the ECHOz2 release which is optimized for rotationally symmetric geometries based on a TE/TM conformal scheme with finite conductivity [26], while the CST-WaK solver is an electromagnetic simulator based on finite integration technique [11].

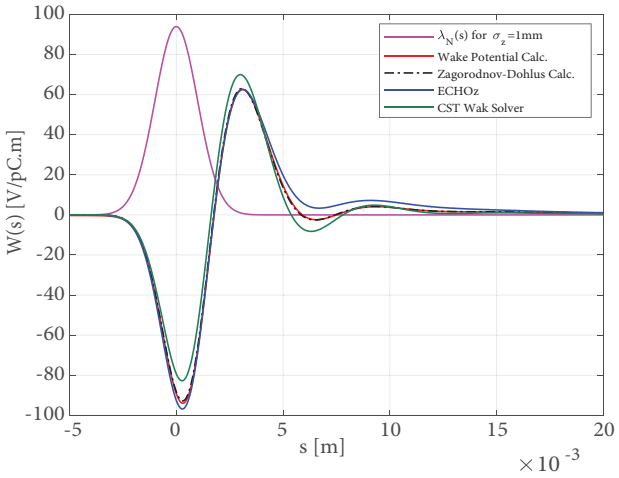

Figure 4. Comparison of the RW Wall Wake potential results.

As it can be seen from Figure 4, a very good match between two analytical calculations and an acceptable degree of consistency with the results of 2D-ECHOz and 3D-CST codes are obtained for the selected simulation parameters. Here we consider a pencil beam with $a \approx 0$ due to limitations of the available codes for the benchmark study. However, for the rest of our numerical calculations the beam radius is considered to be the corresponding value given in Table 1 in order to take into account the contribution of the beam radius to the wakes. We note that λ_N which appears in the following plots indicates the normalized beam charge density.

In Figure 5, we present wake potentials of SNS, JPARC, SIS18, and PS for $0.5m$ and $1m$ bunch lengths in two groups according to range of the variations. The wakes have ≈ 10 larger impact on the bunches for SIS18 and PS compared to SNS and JPARC. This result is consistent with our expectations according to the impedance values given in Table 2. Here we should note that even though the impedance of ECR is slightly larger than that of SNS and JPARC, the wake potential for the ECR is significantly smaller due to its low energy operational characteristic, see Figure 6a. Therefore, one has to take into account not only the impedance but also the energy of the beams to estimate the wake potentials.

We observe larger wakes for shorter bunches in all calculations. Interestingly, the decrease rate of the wake amplitudes are lower for the machines whose wake potentials are the largest, e.g., SIS18 and PS in our parameter scope. Therefore, the wakes could be minimized more efficiently by employing longer bunches in low-impedance and energy machines.

[1]CST (2017). CST Microwave Studio, CST AG Computer Simulation Technology Website https://www.cst.com/ [accessed 06 2017]. (2017) .

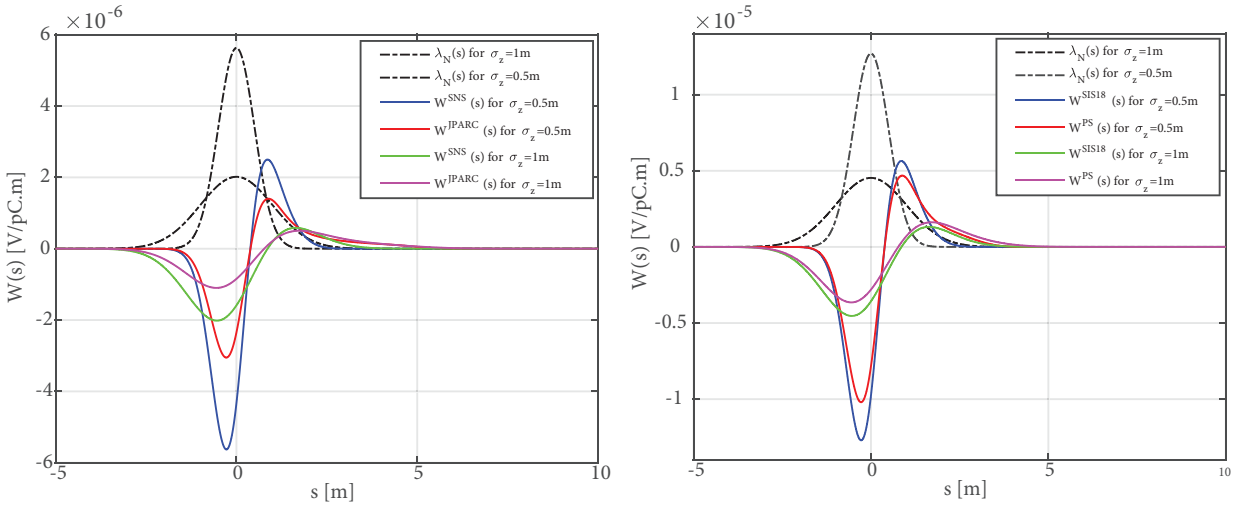

(a) JPARC - SNS (b) SIS18 - PS

Figure 5. Wake potentials for different machines.

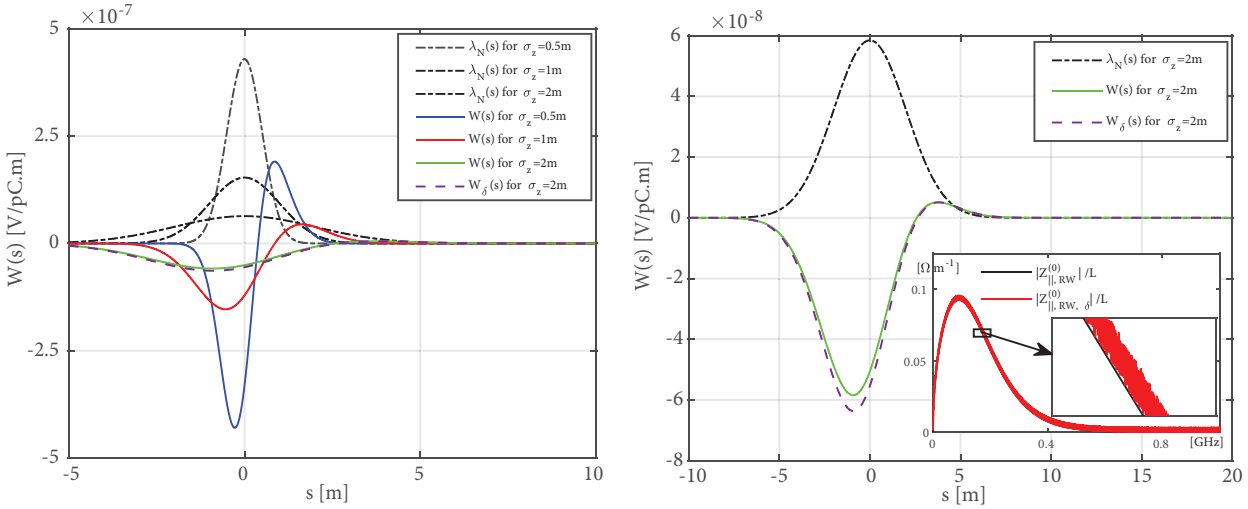

(a) for different bunch lengths (b) from noisy and noise-free impedances

Figure 6. Wake potential of ECR.

In order to observe wake potentials for the noisy impedance data random errors were added pointwise to the analytically calculated impedance data that is,

$$Z^{(0)}_{||,\mathrm{RW},\delta} = Z^{(0)}_{||,\mathrm{RW}} + \xi\,\kappa\,\frac{\|Z^{(0)}_{||,\mathrm{RW}}\|}{\|\kappa\|}\,. \tag{15}$$

Here, $\kappa \in \mathbb{C}$ denotes a random variable with $\{\mathrm{Re}\,\kappa,\ \mathrm{Im}\,\kappa\} \in (0,1)$. The parameter ξ is called the noise ratio and in this study it was chosen as $\xi = 0.05$ to have a noise level of 5%. We illustrate the effect of noisy data in Figure 6b such that $W_\delta(s)$ corresponds to wake potential obtained from noisy impedance data and $W(s)$ is the noise-free wake potential. ECR has the largest wake decrease for long bunches and we used 2 m bunch length in order to determine the effect more clearly. However, the noisy and the exact wake potential values are obtained similarly due to smooth mathematical operators applied in the Fourier transform and convolution.

We note that similar wake potentials are observed from noisy impedances for the other machines and different bunch lengths.

A comparison between the normalized wake potential for different machines is presented in Figure 7 for a $\sigma_z = 1m$ long bunch. The aim of such an illustration is to observe superposed impacts of the parameters given in Table 1 for each machine by focusing on the distributions of the wakes. Wake potentials in JPARC and PS attenuate slower compared to those of SNS, SIS18, and ECR, whose behaviors match well to each other. It is also interesting to see that the ECR has the smallest β, while SIS18/SNS having the largest in the parameter scope the change of their normalized wake potentials are almost identical.

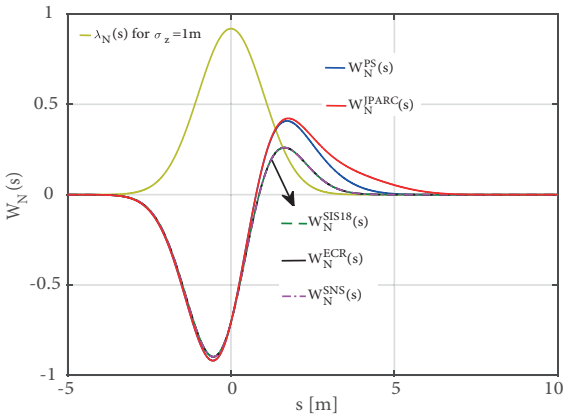

Figure 7. Normalized wake potentials for different machines.

6. Conclusion

In this paper longitudinal resistive wall impedances, wake functions, and wake potentials are calculated numerically over a large scope of β, e.g., $\beta \in \{0.077, \cdots, 0.875\}$, including long $\sigma_z = 0.5m, 1m$ for the Gaussian proton bunched beams passing through a circular cylinder normal conducting beam pipes without pencil beam approximation. The aim of such a wide scope is to cover realistic operating conditions of different accelerator machines and to compare results for different conductivities, beam pipe radii, beam radii, and β.

A wake potential benchmark study using available 2D/3D codes and a different analytical approach which verifies the accuracy of our code is presented. Applicability and the effectiveness of the implemented approach is shown for extreme calculation domains, i.e. the domains for which it is very difficult to obtain accurate results with particle in cell codes.

We note that it can be misleading to estimate the wake behavior of an accelerator only based on impedance distributions and values. Furthermore, it is shown that one has to take into account not only the impedance but also the energy of the beams for wake potential estimations.

This study provides an accurate quantification of impedances and wakes in different scales which might be useful for estimating values for the machines in a similar operation conditions, for benchmark studies of particle in cell codes and for giving some ideas on wake variations with respect to beam and machine parameters.

Acknowledgments

The author would like to thank Fritz Caspers (CERN) for constructive criticism of the manuscript, Michael Plum (SNS) for providing the SNS machine parameters, Igor Zagorodnov (DESY) for his help on the use of

ECHOz, and informing us about the existence of Zagorodnov–Dohlus calculation [24]. Initial studies of this paper are supported by the project BAP-2015-IYTE-32.

References

[1] Zotter BW, Kheifets SA. Impedances and Wakes in High Energy Particle Accelerators. Singapore: World Scientific, 1998.

[2] Boine-Frankenheim O, Gjonaj E, Petrov F, Yaman F, Weiland T et al. Energy loss and longitudinal wakefield of relativistic short proton bunches in electron clouds. Physical Review Special Topics-Accelerators and Beams 2012; 15 (5): 054402. doi: 10.1103/PhysRevSTAB.15.054402

[3] Laslett LJ, Neil VK, Sessler AM. Transverse resistive instabilities of intense coasting beams in particle accelerators. Review of Scientific Instruments 1965; 36 (4): 436-448. doi: 10.1063/1.1719595

[4] Gluckstern RL. Analytic Methods for Calculating Coupling Impedances 2000-011. Meyrin, Switzerland: CERN, 2000.

[5] Zimmermann F, Oide K. Resistive wall wake and impedance for nonultrarelativistic beams. Physical Review Special Topics-Accelerators and Beams 2004; 7 (4): 044201. doi: 10.1103/PhysRevSTAB.7.044201

[6] Zimmermann F, Oide K. Resistive wall wake and impedance for non-ultrarelativistic beams. In: Particle Accelerator Conference (PAC 2003); Portland, OR, USA; 2003. pp. 2604-2606.

[7] Al-Khateeb AM, Boine-Frankenheim O, Hofmann I, Rumolo G. Analytical calculation of the longitudinal space charge and resistive wall impedances in a smooth cylindrical pipe. Physical Review E 2001; 63 (2): 026503. doi: 10.1103/PhysRevE.63.026503

[8] Mounet N. The LHC transverse coupled-bunch instability. PhD, École Polytechnique Fédérale de Lausanne (EPFL), Lausanne, Switzerland, 2012.

[9] Quatraro D, Rumolo G. Non relativistic resistive wall wake fields and single bunch stability. In: 23rd Particle Accelerator Conference (PAC09); Vancouver, BC, Canada; 2009. pp. 3217-3219.

[10] Quatraro D. Collective effects for the LHC injectors: non-ultrarelativistic approaches. PhD, Bologna University, Bologna, Italy, 2011.

[11] Hänichen L, Mueller W, Weiland T, Al-Khateeb AM, Boine-Frankenheim O. Comparison of analytical and numerical results for broadband coupling impedance. In: 23rd Particle Accelerator Conference (PAC09); Vancouver, BC, Canada; 2009. pp. 3420-3422.

[12] Al-Khateeb AM, Boine-Frankenheim O, Hasse RW, Hofmann I. Longitudinal impedance and shielding effectiveness of a resistive beam pipe for arbitrary energy and frequency. Physical Review E 2005; 71 (2): 026501. doi: 10.1103/PhysRevE.71.026501

[13] Zannini C, Rumolo G, Rijoff T, Biancacci N. Electromagnetic simulations for non-ultrarelativistic beams and applications to the cern low energy machines. In: International Particle Accelerator Conference (IPAC2014); Dresden, Germany; 2014. pp. 1718-1720.

[14] Macridin A, Spentzouris P, Amundson J. Impedances and Wake Functions for Non-ultrarelativistic Beams in Circular Chambers Fermilab-Pub-12-518-CD. Batavia, IL, USA: FERMILAB, 2012.

[15] Métral E, Argyropoulos T, Bartosik H, Biancacci N, Buffat X et al. Beam instabilities in hadron synchrotrons. IEEE Transactions on Nuclear Science 2016; 63 (2): 1001-1050. doi: 10.1109/TNS.2015.2513752

[16] Zagorodnov I, Schuhmann R, Weiland T. Long-time numerical computation of electromagnetic fields in the vicinity of a relativistic source. Journal of Computational Physics 2003; 191(2): 525-541. doi: 10.1016/S0021-9991(03)00329-2

[17] Zagorodnov I, Schuhmann R, Weiland T. Conformal FDTD-methods to avoid time step reduction with and without cell enlargement. Journal of Computational Physics 2007; 225 (2): 1493-1507. doi: 10.1016/j.jcp.2007.02.002

[18] Al-Khateeb AM, Hasse R, Boine-Frankenheim O. Comparison of the longitudinal coupling impedance from different source terms. Nuclear Instruments and Methods in Physics Research Section A: Accelerators, Spectrometers, Detectors and Associated Equipment 2008; 593 (3): 171-176. doi:10.1016/j.nima.2008.05.011

[19] Henderson S. SNS Parameters List SNS-100000000-PL0001-R13. Oak Ridge, TN, USA: ORNL, 2005.

[20] Plum MA. Private Communication on SNS Parameters, 2017.

[21] Yaman F, Gjonaj E, Weiland T. 3D EM PIC code to study E-cloud effects for short bunches ($< 50ns$). In: CERN-GSI Electron-Cloud Workshop; Meyrin, Switzerland; 2011.

[22] Franczak B. SIS Parameter List GSI-SIS-TN/87-13. Darmstadt, Germany: GSI, 1987.

[23] Danilov V, Cousineau S, Aleksandrov A, Assadi S, Blokland W et al. Accumulation of high intensity beam and first observations of instabilities in the SNS accumulator ring. In: 39th ICFA Advanced Beam Dynamics Workshop HB2006; Tsukuba, Japan; 2006. pp. 59-63.

[24] Zagorodnov I, Dohlus M. Steady-State Resistive Wake with Oxid Layer and Roughness, Start to End Simulations (S2E). Hamburg, Germany: DESY, 2008.

[25] Zagorodnov I. Wakefield Code ECHO 2(3)D. In: ICFA mini-Workshop on Electromagnetic Wake Fields and Impedances in Particle Accelerators; Erice, Sicily, Italy; 2014.

[26] Zagorodnov I. Computation of electromagnetic fields generated by relativistic beams in complicated structures. In: North American Particle Accelerator Conference (NAPAC'16); Chicago, IL, USA; 2016. pp. 642-646.